



## ORIGINAL RESEARCH

# Maximum current injection method for grid-forming inverters in an islanded microgrid subject to short circuits

Jaume Miret<sup>1</sup>  | Miguel Castilla<sup>1</sup>  | Manel Velasco<sup>2</sup> | Ramón Guzmán<sup>2</sup> | Luis García de Vicuña<sup>1</sup>

<sup>1</sup>Electronic Engineering Department, Technical University of Catalonia, Vilanova i la Geltrú, Spain

<sup>2</sup>Automatic Control Department, Technical University of Catalonia, Vilanova i la Geltrú, Spain

## Correspondence

Jaume Miret, Electronic Engineering Department, Technical University of Catalonia, Vilanova i la Geltrú 08800, Spain.  
Email: jaume.miret@upc.edu

## Funding information

Ministerio de Ciencia y Tecnología, Grant/Award Number: I+D+i PID2021-122835OB-C21

## Abstract

In islanded microgrids, when a short circuit or a sudden overload occurs, it provokes an abrupt increment in the currents supplied by the generation nodes, which feed the load collaboratively. This is particularly challenging for inverter-based nodes, due to its reduced power capacity. This work takes advantage of the droop-method basic configuration to propose an additional closed-loop control, which ensures maximum current injection during any kind of short circuit maintaining the underlying droop control. Ensuring that any node injects its maximum rated current during the short circuit, it emulates the most common low-voltage ride-through protocols for grid-feeding sources oriented to support the grid and, in this way, the voltage unbalance is reduced. To develop the control proposal, a model of the faulted system is presented in order to evaluate the stability of the closed-loop system. A general modelling methodology is introduced in order to derive the control for any microgrid configuration. Finally, selected experimental results are reported in order to validate the effectiveness of the proposed control.

## 1 | INTRODUCTION

Thanks to the advances in power electronics [1] and in the regulatory framework [2], small-scale distributed generation sources (DGS) interfaced to the grid via power converters are becoming ubiquitous. During severe network disturbances, that is, voltage sags, international standards and national grid codes require the continuous operation of grid-feeding DGS (working as power controlled current sources) to avoid cascade disconnections that could lead to severe blackouts [3–6]. In this case, a mature state-of-the-art bibliography deals with the self-protection of grid feeding current-sources against over voltages due to voltage sags [7–11].

When some DGS are islanded from the main grid forming a microgrid, the whole system may suffer from more severe challenges when dealing with sags and overcurrents, due to its reduced power capacity. On the one hand, the nodes of the microgrid that are synchronous machines can deal with relatively high overcurrents; on the other hand, inverter-based nodes have more restrictive overcurrent ratings in amplitude and duration. These restrictions can compromise its function-

alities as voltage sources, and in the worst-case scenario, allow it to disconnect. The simpler approach to avoid overcurrents in an inverter-based power converter is the saturation of the reference input in the current loop, which produces distortion and most importantly, could bring an instability to the system [12–14], particularly when feeding an islanded microgrid.

### 1.1 | Comprehensive state-of-the-art comparison

First, it must be noted that in the field of islanded microgrids there are only a few works dealing with current limiting controllers for grid-forming converters. These are few compared with the vast number of references, and also grid-codes, regarding the grid-feeding converter's behaviour under overcurrents or voltage sags. Secondly, in the author's opinion, this topic should deserve more attention from the experts due to the increasing penetration of inverters in islanded systems. Without high-performance overcurrent controls in the power converters, an islanded microgrid under these faults would tend to cause

This is an open access article under the terms of the [Creative Commons Attribution-NonCommercial-NoDerivs](https://creativecommons.org/licenses/by-nc-nd/4.0/) License, which permits use and distribution in any medium, provided the original work is properly cited, the use is non-commercial and no modifications or adaptations are made.

© 2023 The Authors. *IET Power Electronics* published by John Wiley & Sons Ltd on behalf of The Institution of Engineering and Technology.

a cascade leading to a blackout, instead of preserving rough voltage regulation and ensure power delivery to the loads.

In the field of islanded microgrids, some works propose changing the current loop to avoid overcurrents during a fault [15–17]. They introduce fault detection/protection methods based on limiting the amplitude of the reference current, thus changing the operation from grid-forming to grid-feeding. In addition, these methods must include anti-windup strategies to avoid the saturation of the outer voltage loop.

To avoid this drawback, the most promising methods to deal with overcurrents in a microgrid include different approaches based on adding/changing virtual impedances during the disturbance [18–23]. All these works share a common disadvantage: the maximum allowable current injection  $I_{rated}$  is not ensured due to the fact that the operation depends highly on unknown short circuit and system parameters.

The work in [18] presents a simple switching open-loop control, which calculates the virtual parallel impedance that reduces the output current in case of there being an unbalanced short circuit for a stand-alone inverter. In [19], the insertion of a virtual resistance in series with the inverter output was proposed, in order to reduce the output voltage when the maximum allowed current is reached. It requires an exact knowledge of the load and is valid only for balanced overloads. In [20] and [21], the conventional virtual output impedance is enhanced with a proportional term that depends on the overcurrent magnitude, although it does not provide maximum current. In [22], the current reference of a grid-connected inverter is calculated on-line to limit the maximum current during unbalanced short circuits. In parallel, an adaptive virtual impedance, proportional to the fault severity, reduces the output voltage reference. Due to its implementation, complex interactions appear between the two parallel controls, which make it difficult to ensure the system stability in an islanded microgrid. In [23], a virtual impedance in phase with the droop-control virtual-impedance is connected during a fault in an islanded microgrid.

A few works deal with overcurrent controllers without adding virtual impedances [24–27]. The work presented in [24] proposes a proportional controller that adds some amount of  $d$ -axis output voltage amplitude to the power/frequency ( $P/f$ ) loop, which is non-zero during a short circuit. The main drawback is that, during unbalanced sags, voltage amplitudes in dq frame present oscillations, which add distortion to the  $P/f$  loop. In addition, the proportional parameter design limits the application of the control to known ranges of both current and line impedances. In [25], synchronous power control is used to drive a lone grid-connected inverter. During the short circuit, the active and reactive power references obtained by the conventional droop method are switched to a fault mode reference control which computes new power references. The main disadvantage of this proposal is that it is only useful for symmetric short circuits. In [26] and [27] switched controllers impose maximum currents in the faulty phases. In [26] the initial overcurrent is avoided by clamping the currents and in [27] using a hysteresis comparator-based hardware limiter. The main drawback of both controllers is the switched control that allows the conventional voltage plus current loops to

become uncontrolled, which can negatively affect the system stability.

Table 1 summarizes the main features of the previous controllers when dealing with overcurrents, with the last column listing its experimental verification, being HIL the acronym of the hardware in the loop.

## 1.2 | Contributions to the state-of-the-art

This work proposes a protection scheme that overcomes the limitations of previous works. The most relevant feature of the controller presented in this paper is that, during any kind of short circuit, maximum current injection is always reached and the reduction of the voltage unbalance is ensured. Injecting the maximum allowable current is the requirement of some grid codes to grid-feeding DGS when dealing with low-voltage-ride-through scenarios. The proposal here mimics these grid codes for grid-forming DGS in an islanded microgrid. In this way, it provides maximum support to the microgrid while maintaining its functionalities as a grid-forming converter. The main contribution of this work is a control scheme that meets three interesting features, not fulfilled together in any of the previous works. These features are:

- (i) It maintains the grid-forming characteristics of the inverter without requiring additional fault operation mode.
- (ii) It provides exactly the maximum allowable current  $I_{rated}$ , that is, it mimics the grid code requirements for grid-feeding converters during low-voltage-ride-through protocols [2–4].
- (iii) Previous feature results in a reduction in the voltage unbalance.
- (iv) A general modelling methodology is introduced in order to derive the control for any microgrid configuration.

The last line of Table 1 lists the main features of the proposal compared with the state-of-the-art control solutions. The paper is organized as follows. Section 2 models the microgrid grid-forming inverters under short circuit. Section 3 presents the control objectives and the design guidelines to obtain the controller and its parameters. Section 4 corroborates experimentally the expected features. Section 5 concludes the work.

## 2 | MODELLING GRID-FORMING INVERTERS UNDER SHORT CIRCUITS

This section introduces the model of a grid-forming inverter connected to a faulted load using its positive- and negative-sequence equivalent circuits.

### 2.1 | Droop control of islanded microgrids

Commonly, in the hierarchical control of microgrids, the primary layer is based on a local controller that ensures active and

**TABLE 1** Comparison with state-of-the-art techniques

Ref.	$I_{rated}$	$\mu grid$	Island operat.	Unbalan. faults	Voltage unbalan. reduction	Switch control	Experim. results
[18]	✗	✗	✓	✓	✗	✗	✓
[19]	✗	✓	✓	✓	✗	✗	HIL
[20, 21]	✗	✓	✓	✗	✗	✗	✓
[22]	✓	✗	✗	✓	✗	✗	✗
[23]	✓	✓	✓	✓	✗	✗	HIL
[24]	✗	✓	✓	✗	✗	✗	HIL
[25]	✓	✗	✗	✗	✗	✗	✓
[26]	✓	✓	✓	✓	✗	✓	✗
[27]	✓	✓	✓	✓	✗	✓	✓
Prop.	✓	✓	✓	✓	✓	✗	✓

reactive power sharing between grid-forming nodes [28]. The references for the angular frequency  $\omega^*$  and the amplitude  $V^*$  of the voltage generated by each DG can be derived using the droop method [29]

$$\omega^* = \omega_o - mP \quad (1)$$

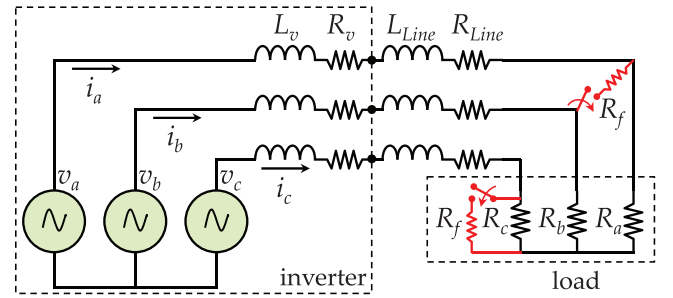
$$V^* = V_o - nQ \quad (2)$$

where  $\omega_o$  is the nominal angular frequency,  $m$  is the droop coefficient for active power,  $P$  is the mean value of the exported active power,  $V_o$  is the nominal voltage,  $n$  is the droop coefficient for reactive power and, finally,  $Q$  is the mean value of the exported reactive power. Conventionally,  $P$  and  $Q$  are obtained filtering its instantaneous values with a low pass filter, tuned at  $\omega_{LPQ} = 0.1 \cdot 2 \cdot \omega_o$ , to attenuate oscillations at twice the grid frequency [28, 30]. In addition to (1) and (2), a virtual impedance is commonly added to enhance the controllability when using the droop method [20]. Finally, the reference voltage provided to the voltage loop is expressed as [30]

$$v^*(t) = V^* \sin(\omega^* \cdot t) - R_v i(t) - L_v \frac{di(t)}{dt}. \quad (3)$$

being  $R_v$  and  $L_v$  the output virtual resistance and inductance set by the designer, and  $i(t)$  the output current provided by the inverter.

A method to model the behaviour of the microgrid and the different DGs is to consider individual inverters (henceforth also named as microgrid nodes) connected to a bus where the load is wired, with the other nodes being considered perturbations [31]. Each node can be modelled as a voltage source with its virtual output impedance  $Z_v$  ( $R_v + j\omega L_v$ ) in series with the line impedance  $Z_{Line}$  and, finally the load  $R$ , as shown in Figure 1. Commonly, the connection between the inverter and the line must be isolated, and thus, the impedance of the required output transformer is included in  $Z_{line}$ . In normal conditions, assuming a balanced wye-connected resistive load (equal

**FIGURE 1** Simplified diagram of a three-phase inverter under different short circuits

resistance in each phase, i.e.  $R_a = R_b = R_c = R$ ), the three-phase current (in Laplace domain) that provides the particular inverter is

$$\mathbf{i}_{abc} = (\mathbf{I} \cdot \mathbf{Z}_t)^{-1} \cdot \mathbf{v}_{abc} \quad (4)$$

$$\mathbf{Z}_t = \mathbf{Z}_v + \mathbf{Z}_{line} + \mathbf{R} \quad (5)$$

where  $\mathbf{I}$  is the  $3 \times 3$  identity matrix.

## 2.2 | Short circuit types and simulation example

In this generalized scheme, a short circuit is commonly modelled as a fault resistance  $R_f$  connected between a line and the load virtual-ground (line-to-ground fault) or between lines (line-to-line fault), as shown in Figure 1 [32]. Both types of short circuits generate an unbalanced voltage sag in the microgrid. In addition, a third type of short circuit is observed when a line-to-ground fault occurs in the three phases simultaneously, with the same  $R_f$ , thus causing a balanced voltage sag.

In previous works [20, 21, 24, 25], only balanced short circuits were considered (i.e. an equal per phase reduction of the load

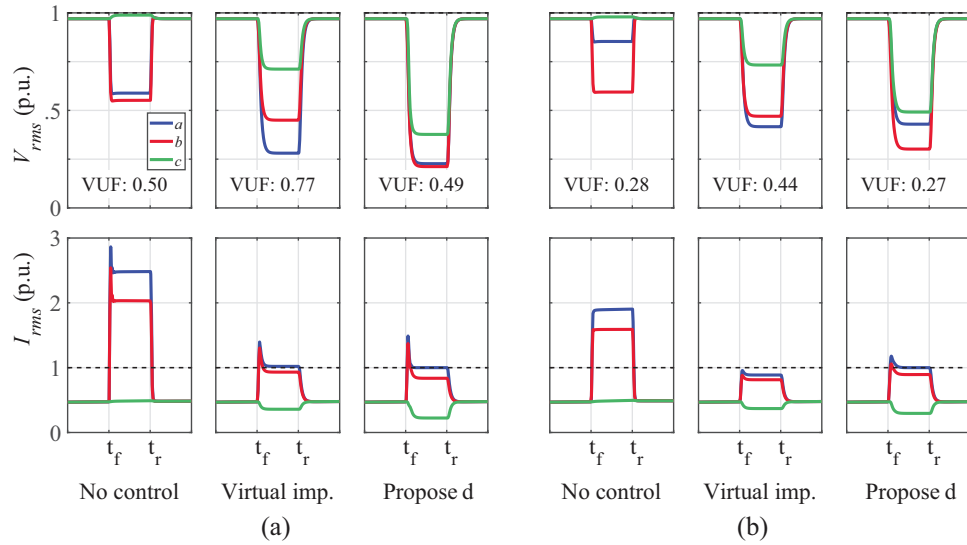


**FIGURE 2** Simulation of a two-inverter-based microgrid under a line-to-line short circuit. (a) With  $R_f = 0 \Omega$ , the most severe short circuit, (b) with  $R_f = 11 \Omega$ , less severe short circuit. Phase voltages and currents of inverter 1

value  $R$  in Figure 1). It is worth mentioning that in the present work all kinds of short circuits are considered and, therefore, their consequences can be adequately handled by a specifically designed control system, as seen below.

Figure 2 shows the simulation results of a microgrid with two droop-controlled inverters ( $Z_{v1,2} = 0 + j2.2 \Omega$ ,  $Z_{line1} = 0.5 + j4.7 \Omega$ ,  $Z_{line2} = 0.6 + j1.9 \Omega$ ), feeding a common load ( $V_o = 155 \text{ V}$ ,  $R = 12 \Omega$ ), under different short circuit resistor values connected between phase  $a$  and phase  $b$ , starting at time  $t = t_f$  and recovering at  $t = t_r$ . It depicts the root mean square values (RMS) of phase output-voltages and currents of one of the inverters. Figure 2a shows the system suffering a severe short circuit, with  $R_f = 0 \Omega$ . As can be seen, before the short circuit, the inverter is supplying 0.5 p.u. per phase current. During the fault, when no additional short circuit control is implemented (i.e. using only droop-control (1) to (3)), phase  $a$  and  $b$  currents exceed 2 p.u., obviously yielding its disconnection in a real system. Even worse, the inverter controller generates

only balanced reference voltages through (1) and (2), and the presence of the virtual impedance  $Z_v$  induces voltage unbalance in the inverter output. In this case, the voltage unbalance factor (VUF) is increased from 0 to 0.5 during the fault. The VUF value is defined as the quotient between the negative and positive sequence amplitudes [6].

When using state-of-the-art virtual impedance controllers [18–21], if the impedance value is correctly determined for this most severe case, the phase currents are successfully reduced to the maximum allowable current, that is,  $I_{rated} = 1 \text{ p.u.}$

These controllers are based on increasing the virtual output impedance  $Z_v$  in (3) during the short circuit. Of course, due to this increase, the phase voltages are reduced to trying to maintain the active power required by the loads, with the voltage unbalance highly increased from  $VUF = 0.5$  to 0.77.

When simulating the proposal of this work, the highest phase current is limited to  $I_{rated}$ . In this case both controllers (state-of-the-art virtual output impedance and proposal) work

successfully protecting the inverter and avoiding the cascade black-out. As can be seen, the voltage unbalance is reduced to  $VUF = 0.49$  when using the proposal compared with the conventional approach (virtual impedance). This issue is due because the higher current is injected to the phase with the most reduced voltage.

Figure 2b shows the same microgrid during a less severe short circuit,  $R_f = 11 \Omega$ . As can be seen, when using virtual impedance control, the currents are safely confined although clearly below the maximum  $I_{rated}$  value.  $I_{rated}$  is not reached because the virtual impedance controllers are based on proportional gains adjusted for the worst-case condition. When using the proposal, it can be seen that phase  $a$  current is exactly  $I_{rated}$ . This interesting feature is the main advantage

of this work's proposal, that is, the injection of maximum current through the most faulted phase ensures that the inverter maximizes its effort to support the entire system, similarly to the requirements in grid-feeding systems [2–4].

Consequently, the VUF is highly reduced when comparing the results with the conventional controller (from 0.44 to 0.27).

It must be noted that line-to-line short circuits cause higher overcurrents than line-to-ground short circuits. For example, in Figure 2a, the maximum short circuit current occurs in phase  $a$  and takes a value of 2.5 p.u. In a phase-to-ground short circuit with the same characteristics ( $R_f = 0 \Omega$ ), the maximum short circuit current is 1.3 p.u. when no control is applied.

### 2.3 | Symmetric positive and negative model, overcurrent modelling

The mathematical expression of the current supplied by each phase must be determined in order to derive a controller to avoid overcurrents and ensure the system stability.

For line-to-line fault, the load and the fault resistance  $R_f$  seen in Figure 1 can be transformed easily to an unbalanced load,

from three equal  $R$  to a new equivalent resistance per each phase  $R_a$ ,  $R_b$  and  $R_c$ .

$$R_a = \frac{R \cdot R_f}{2R + R_f} \quad R_b = \frac{R \cdot R_f}{2R + R_f} \quad R_c = \frac{3R^2 + R \cdot R_f}{2R + R_f} \quad (6)$$

Also the total impedance  $Z_l$  in (5) is different for each phase ( $Z_{la}$ ,  $Z_{lb}$  and  $Z_{lc}$ ), thus (4) becomes

$$\begin{bmatrix} i_a \\ i_b \\ i_c \end{bmatrix} = A \cdot \begin{bmatrix} -Z_{lb} - Z_{lc} & Z_{lc} & Z_{lb} \\ Z_{lc} & -Z_{ta} - Z_{tc} & Z_{ta} \\ Z_{lb} & Z_{ta} & -Z_{ta} - Z_{lb} \end{bmatrix} \cdot \begin{bmatrix} v_a \\ v_b \\ v_c \end{bmatrix} \quad (7)$$

$$A = \frac{1}{Z_{la}Z_{lb} + Z_{ta}Z_{lc} + Z_{lb}Z_{tc}}. \quad (8)$$

It must be noted that, with load imbalance, the admittance matrix  $Y_{abc}$  in (7) takes different values in the main diagonal and also values that can be different from zero elsewhere. Thus, the current provided by each phase depends on its phase voltage but also on the other two phase voltages. To simplify the modelling avoiding this cross-coupling, the three-phase system composed by the inverter, the line and the load can be described with symmetric components using the Fortescue theorem [32]. Via this theorem, (7) can be expressed in symmetric zero, positive, and negative sequences as

$$i_{0pn} = Y_{0pn} \cdot v_{0pn} \quad (9)$$

where the sequences matrix is obtained as

$$Y_{0pn} = F \cdot Y_{abc} \cdot F^{-1} \quad (10)$$

with the phasor rotation operator matrix  $F$  defined as

$$F = \begin{bmatrix} 1 & e^{j\frac{2\pi}{3}} & e^{j\frac{4\pi}{3}} \\ 1 & e^{j\frac{4\pi}{3}} & e^{j\frac{2\pi}{3}} \\ 1 & 1 & 1 \end{bmatrix}. \quad (11)$$

Considering a three-wire node connected to the line by wye-delta output-transformers, that is, without zero sequence, only the positive and negative sequences must be taken into account, and thus (9) is reduced to a  $2 \times 2$  positive and negative sequences system. In addition, only positive sequence voltage  $v_p = v$  is generated by the reference voltage in the droop method, zero being the negative sequence reference  $v_n = 0$ . Then, the positive and negative sequence currents,  $i_p$  and  $i_n$ , can be determined

$$\begin{bmatrix} i_p \\ i_n \end{bmatrix} = Y_{pn} \cdot \begin{bmatrix} v \\ 0 \end{bmatrix} = \begin{bmatrix} Y_{11} & Y_{12} \\ Y_{21} & Y_{22} \end{bmatrix} \cdot \begin{bmatrix} v \\ 0 \end{bmatrix}. \quad (12)$$

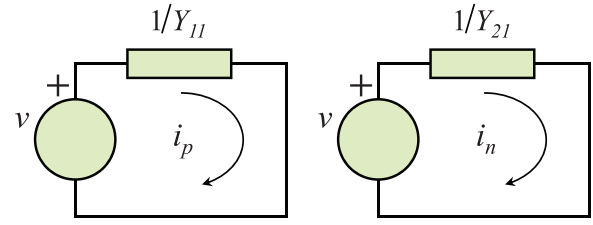


**FIGURE 3** Inverter model separated into positive and negative sequence circuits

As described above, due to load imbalance, all the elements of  $Y_{pn}$  are different from zero, and thus, negative sequence current flows from the inverter output (modelled in Figure 3). It must be noted that the elements of  $Y_{pn}$  are expressed in the Laplace domain and have complex coefficients, due to the phasor rotation (11). As can be seen, the models for the positive and the negative circuits are decoupled, as desired (see Figure 3).

In order to obtain the expressions of the phase currents, the last step is to compute the phase current amplitudes using the positive/negative model of Figure 3

$$I_a = |(Y_{11} + Y_{21} e^{j0})v| \quad (13)$$

$$I_b = \left| \left( Y_{11} e^{-j\frac{2\pi}{3}} + Y_{21} e^{j\frac{2\pi}{3}} \right) v \right| \quad (14)$$

$$I_c = \left| \left( Y_{11} e^{j\frac{2\pi}{3}} + Y_{21} e^{-j\frac{2\pi}{3}} \right) v \right|. \quad (15)$$

Finally, the transfer function that models the behaviour of the maximum phase amplitude, due to the overcurrent, is easily determined from these expressions

$$I_{max} = \max \{I_a, I_b, I_c\}. \quad (16)$$

Generalizing (16) for a particular inverter  $i$ , it can be seen that the maximum current amplitude depends linearly on the amplitude  $V$  and on the equivalent admittance  $Y_i$  seen by the inverter

$$I_{max\_i} = Y_i \cdot V. \quad (17)$$

This observation is supported by the fact that the voltage  $v$  is a multiplying factor in the three amplitudes expressed in (13)–(15).

## 2.4 | Microgrid modelling procedure

As explained above, different inverters are wired together to feed collaboratively the common loads of a microgrid. To obtain a full mathematical model of a microgrid, the line parameters are commonly estimated, using values of line and load impedances that would differ from the real values. Also, and most important, it must be noted that the inverters work simultaneously,



and some of them can be connected or disconnected randomly, sharing the same local control objectives. In general, obtaining a full mathematical model of a real microgrid would be useless for designing the control system due to these uncertainties.

In this work, the system modelling will follow a different approach. It is based on obtaining a reduced plant for each inverter, and then deriving a family of plants  $Y_{family}(s)$ , that encompasses all the system uncertainties around a nominal plant  $Y_{nominal}(s)$ . The reduction technique chosen here models each inverter preserving the low-frequency dynamics when it operates in an islanded microgrid [33, 34]. The reduced models will facilitate the controller derivation using the well-known robust control design methodology [35–37]. Finally, to ensure that the design is correct it is required to apply a robust stability test to the closed-loop system.

The first step in this modelling technique is to particularize the linear transfer function (17) for each inverter under different fault conditions and to reduce it to a first-order system [33].

Second, in order to apply robust control design and taking into account the uncertainty inherent in the set of reduced plants, the nominal plant  $Y_{nominal}(s)$  (with minimum difference with the rest of the plants) and the additive uncertainty model  $\omega_u^a(s)$  around the nominal plant must be determined [36].

At last, a new function,  $Y_{family}(s)$ , must be defined as the enveloping function that considers the complete set of plants and also the infinite plants comprised inside the uncertainty region [37]

$$Y_{family}(s) = Y_{nominal}(s) + \omega_u^a(s) \cdot \Delta(s) \quad (18)$$

where  $\omega_u^a(s)$  must be chosen larger than any difference at any frequency between any modelled plant and the nominal plant. The complex number  $\Delta(s)$  (such that  $|\Delta(j\omega)| \leq 1$ ) ensures that any plant is inside the defined family envelope.

Summarizing, instead of obtaining a full mathematical model of the microgrid, that in a real scenario would be useless for designing the control system due to parameter uncertainties and unknown presence/absence of some inverters, the microgrid linear model in (18) encompasses the uncertainty of a real system.

## 2.5 | Laboratory microgrid model

As an example, the modelling procedure described above is applied to the experimental setup schematized in Figure 4. It should be noted that this is a general procedure and can be applied to any particular microgrid configuration.

A three-phase four-feeder microgrid experimental setup is considered in this paper, which is composed of six inverter-based DG nodes (#1–#6 in Figure 4). Each DG acts as a grid-forming node, that is, it operates as a power-controlled voltage source, coupled to the microgrid through a 1:1 wye-delta isolation transformer. The six nodes feed collaboratively a global load  $L_{Bus4}$ . The short circuit occurs in this load. The

data shown in Figure 4 and the parameters defined in Table 2 have been used to model the experimental setup.

Each inverter is modelled as Figure 1 shows, particularizing the transfer function (17) with its virtual impedance, its line impedance until reaching the fault and the fault resistor listed in Table 2. To particularize the model to the fault, a line-to-line fault has been chosen because higher currents are expected in this case, as presented in Section 2.2. On the one hand, the worst case, that is, which causes maximum overcurrent, is a line-to-line fault with  $R_f$  equal to zero. On the other hand, the minimum overcurrent that triggers the controller occurs when the fault resistance value  $R_f = R_{f\_max}$  causes a current equal to  $I_{rated}$ . Taking into account these two cases, two extreme equivalent plant functions are derived for each node. As can be seen, a new uncertainty has appeared, the value of the fault resistance  $R_f$  and the fault location. At last, these two plants are reduced to a first-order system, although preserving the inverter low-frequency dynamics. Thus, 12 plant models are obtained for the microgrid shown in Figure 4, see the appendix for a detailed description.

Finally, using this set of 12 plants, the nominal plant  $Y_{nominal}(s)$  and the additive uncertainty model  $\omega_u^a(s)$  are determined to obtain the family of plants  $Y_{family}(s)$  in (18). The mathematical description of the nominal plant and the additive uncertainty for the proposed microgrid are also reported in the appendix.

## 3 | PROPOSED CONTROL AND DESIGN GUIDELINES

### 3.1 | Control objective and proposal

The main objective of this work is to ensure that, during the short circuit, the inverter injects its maximum rated current amplitude  $I_{rated}$  without clamping the current and voltage waveforms. Additionally, this objective should be reached while the grid-forming control scheme based on the droop method is maintained, also during the fault. Then, the proposed main objective of this work is defined as

$$I_{max} = I_{rated} \quad (19)$$

State-of-the-art control approaches are based on adding some resistive value to the virtual impedance  $Z_v$  during the disturbance [18–22]. Of course, as demonstrated in these works, the increase of the resistive value of  $Z_v$  reduces the output current. Although, the shared objective in these works is less ambitious than (19), that is

$$I_{max} \leq I_{rated} \quad (20)$$

works, the increase of the resistive value of  $Z_v$  reduces the output current. Although, the shared objective in these works. However, as seen in (13)–(16), the virtual impedance (presented in  $Y_{11}$  and  $Y_{22}$ ) has a complex non-linear effect in  $I_{max}$ , and, thus, it is difficult to counteract exactly any perturbation profile varying  $Z_v$ .

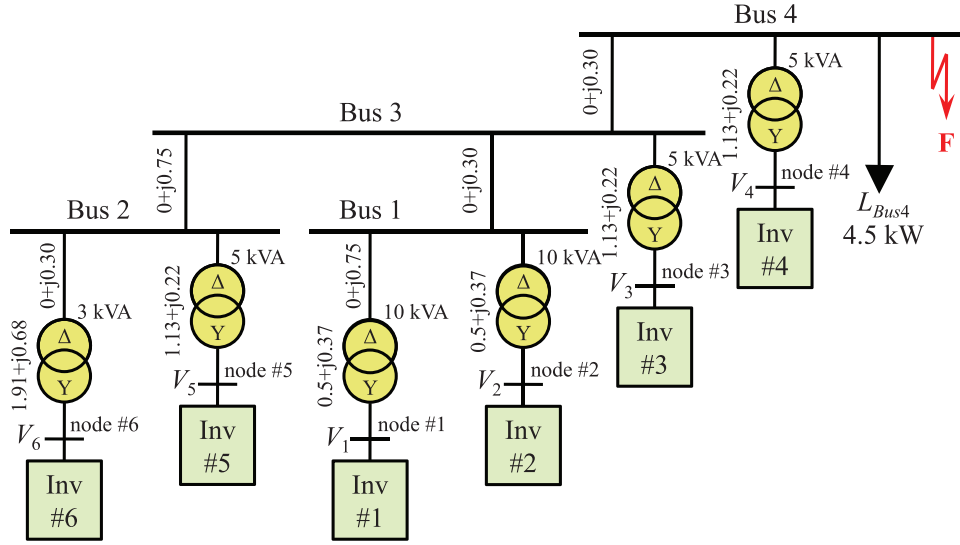


FIGURE 4 Single-line schematic diagram of the microgrid under study

TABLE 2 Microgrid electric and control parameters

Parameter name	Acronym	Value	Units
Nominal voltage	$V_o$	155	V
Nominal frequency	$f_o$	60	Hz
$P$ and $Q$ low pass filter freq.	$\omega_{LPQ}$	12	Hz
Rated current amplitude	$I_{rated}$	10	A
Frequency droop param.	$m$	1	mrad/Ws
Voltage droop parameter	$n$	50	$\mu V/VAr$
Nominal load per phase	$R$	8	$\Omega$
Short circuit resistor (min.)	$R_{f\_min}$	0	$\Omega$
Short circuit resistor (max.)	$R_{f\_max}$	2	$\Omega$
Virtual impedance	$Z_v$	$0.0 + 1.0j$	$\Omega$
Line impedance inverter #1	$Z_{Line1}$	$0.5 + 1.7j$	$\Omega$
Line impedance inverter #2	$Z_{Line2}$	$0.5 + 0.9j$	$\Omega$
Line impedance inverter #3	$Z_{Line3}$	$1.1 + 0.5j$	$\Omega$
Line impedance inverter #4	$Z_{Line4}$	$1.1 + 0.2j$	$\Omega$
Line impedance inverter #5	$Z_{Line5}$	$1.1 + 1.3j$	$\Omega$
Line impedance inverter #6	$Z_{Line6}$	$1.9 + 2.0j$	$\Omega$

Alternatively, the proposal of this work is the direct control of  $V$ , that is, the amplitude of the voltage generated in the inverter in (2). In this case,  $I_{max}$  can be finely adjusted dropping  $V$  adequately since there is a proportional relationship between these two variables, as (17) demonstrates. Figure 5 shows the block diagram of a control proposal that fulfils the control objective in (19) adding a supplementary current loop. The alternative of merging this control loop with the inner voltage and current control loops, or the virtual impedance loop, would provide a more complex implementation. In this way, the analysis and design with this merged solution would be more complex. With

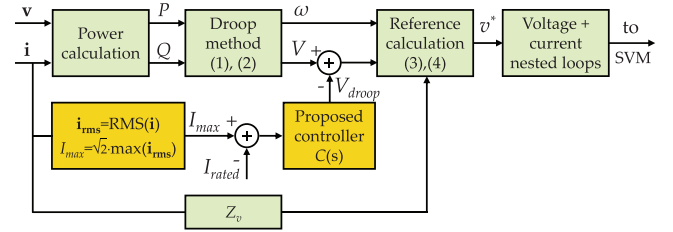


FIGURE 5 Block diagram of the proposed control scheme

the control proposal, based on a supplementary current control loop, the control design is easier, as will be seen below.

The blocks in green correspond to the basic configuration presented in (1)–(3), which feed a conventional voltage/current nested loops and finally a space vector modulator (SVM) to drive the inverter switches. The inner voltage and current control loops are based on conventional control loops with PRES compensators [1].

The proposal (in orange) is based on a linear controller, which determines the necessary droop voltage  $V_{droop}$  in the reference amplitude  $V$  to limit the maximum current to  $I_{rated}$ .  $I_{max}$  is calculated using an algorithm that computes the RMS values of the current vector  $i$  and determines its maximum. The RMS block is based on an integral-sliding window filter, with a window-width of a half grid-period, and modelled as a first-order low pass filter [38]

$$H_{rms}(s) = \frac{2\omega_o}{s + 2\omega_o}. \quad (21)$$

$V_{droop}$  is bounded to zero; thus, it is always present in the whole controller, before the reference calculation block, and activated only by the overcurrent.

This simple configuration avoids the inherent complexities of controls that require switching between normal mode to fault

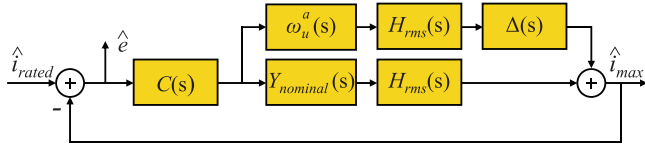


FIGURE 6 Closed-loop model meeting  $H_\infty$  design

mode as done in [26] and [27]. In addition, the synchronization of the inner voltage and current loops is not affected by the action of this voltage amplitude reduction.

### 3.2 | $H_\infty$ controller design methodology

From the microgrid model (18) and taking into account the control scheme in Figure 5, robust control design methodology will be used below to obtain the controller that fulfils the objective (19).

Figure 6 shows the closed-loop model meeting  $H_\infty$  design methodology. From this figure, the sensitivity function  $S(s)$  can be defined, relating the error and the rated current

$$S(s) = \frac{e(s)}{\hat{i}_{rated}(s)}. \quad (22)$$

Thus, a controller  $C(s)$  must be designed to meet the stability criteria [37]

$$|H_{rms}(j\omega) \cdot C(j\omega) \cdot S(j\omega)| < \frac{1}{|\omega_u^a(j\omega)|} \forall \omega. \quad (23)$$

### 3.3 | Design requirements, controller derivation

This subsection introduces a procedure to derive the controller configuration that accomplishes both the control objective (19) and some particular dynamic characteristics. This is a general procedure that can be applied to any microgrid architecture. In this subsection, it is used to devise the proposed control scheme of the microgrid shown in Figure 4.

Two main design requirements were chosen for all the possible plants: first, the accomplishment of the control objective  $I_{max} = I_{rated}$ , that is, DC zero error. Second, to ensure a sufficient stability margin and an adequate transient response. In particular, a minimum phase margin (PM) of  $45^\circ$  and a closed-loop bandwidth (BW) at least of 3 Hz are set by the designer.

The requirements for the closed-loop control can be met defining a weighting function  $\omega_e(s)$  that specifies the maximum boundaries for the sensitivity function. Following [37], different weighting functions that meet the proposed requirements can be calculated. In this work, the chosen weighting function was

$$\omega_e(s) = \frac{0.1175 (s+1200)^2 (s+101)^2}{s (s+257)^3}. \quad (24)$$

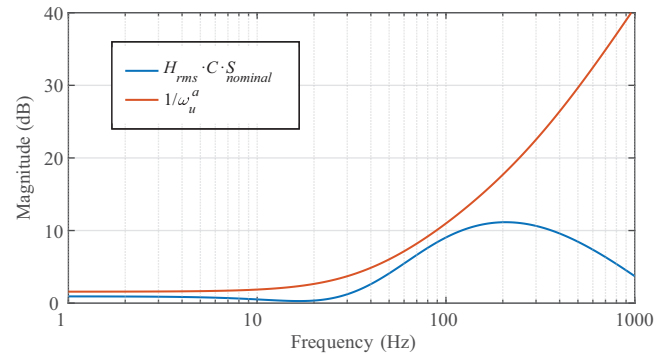


FIGURE 7 Robust stability in (23)

Finally, in order to ensure that the controller meets the design requirement given by the weighting function, the following inequality must be fulfilled [37]:

$$|S(j\omega)| < \frac{1}{|\omega_e(j\omega)|} \forall \omega. \quad (25)$$

MATLAB  $H_\infty$  tools (*H-Infinity Synthesis*) were used to solve the mixed optimization problem of (23) and (25). After this synthesis, the controller can be written as

$$C(s) = \frac{100 \cdot 10^3 (s+402)(s+1833)(s+1900)(s^2+307s+27 \cdot 10^3)}{s (s+1905)(s+240)^2 (s^2+8564s+32 \cdot 10^6)}. \quad (26)$$

It must be noted that the fulfilment of the proposed main objective, that is,  $I_{max} = I_{rated}$ , will be granted by the pole at the origin present in the controller, that is, an integrator. This integrator will provide a smooth change in the inverter current when the fault arrives. The other terms ensure that all the possible plants (inverters) working in parallel will fulfil the chosen stability margin and will have the desired transient response.

Finally, and most important, it must be considered that, when changing the microgrid hardware setup, that is, adding generation nodes, the usefulness of controller (26) must be ensured. To do this, the designer only needs to derive the transfer function (17) for the new inverter and its impedances (see the appendix). If this transfer function is located inside the range of the envelope  $Y_{family}(s)$  (18) the synthesized controller (26) will still be useful for the new setup, and the overall stability will not be compromised. With a fine design of the connection lines of the new node, it is sure that the transfer function (17) will be inside  $Y_{family}(s)$ .

### 3.4 | Stability analysis

As mentioned above, the resulting controller grants stability for all the plants in spite of the considered uncertainties. Figure 7 shows that the controller ensures the fulfilment of the stability criterion for all frequencies because the magnitude



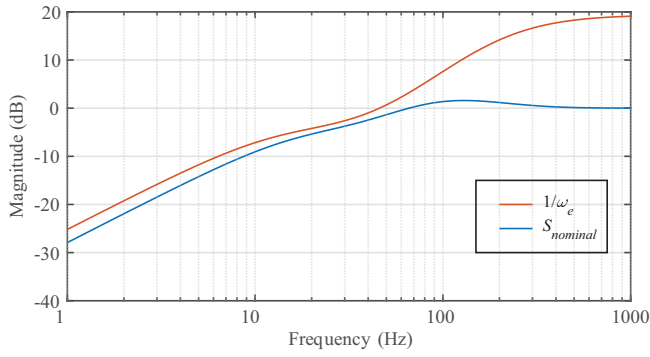


FIGURE 8 Performance criterion in (25)

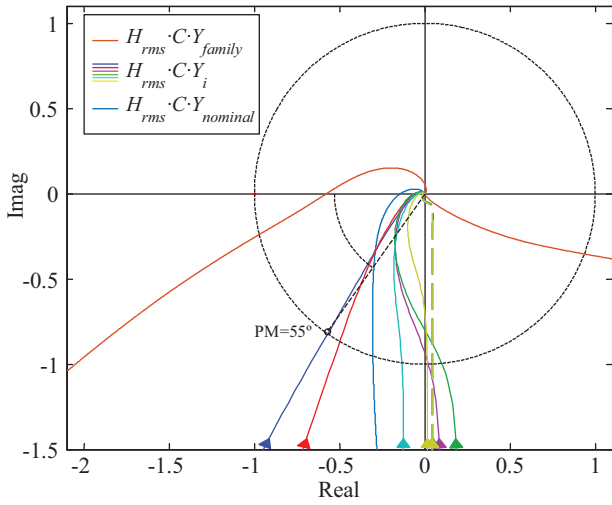


FIGURE 9 Nyquist diagram of the family of plants and nominal plant, in bold red and bold blue, respectively. Diagrams for Inverter #1 in blue, #2 in thin red, #3 in magenta, #4 in green, #5 in cyan and #6 in yellow. Continuous lines for line-to-line faults with  $R_{f\_min}$ , dashed lines for faults with  $R_{f\_max}$ . Minimum PM =  $55^\circ$  for inverter #1 with  $R_{f\_min}$

of  $H_{rms} \cdot C \cdot S(s)$  for the nominal plant (in blue) lies below the modulus of  $1/\omega_e(s)$ , as stated in (23).

The accomplishment of the performance criterion (25) for the nominal plant when using the proposed controller is shown graphically in Figure 8. It can be observed that the modulus of the sensitivity  $S(s)$  of the nominal plant (in blue) lies below the magnitude of  $1/\omega_e(s)$ .

Finally, Figure 9 complements the stability and performance evaluation by showing the Nyquist plot of the loop gains of the uncertain family  $Y_{family}$ , the modelled plants and the nominal plant with the designed controller. All the plants meet the minimum PM requirement. Note that the minimum PM is  $55.3^\circ$ , with a BW of 25.9 Hz, corresponding to inverter #1 line-to-line fault with  $R_{f\_min}$  (clearly higher than the designed minimum PM of  $45^\circ$ ). The five pairs of PM and BW for the other plants with the same fault are: [59.9, 32.7], [90.8, 25.7], [95.7, 27.6], [82.4, 22.2] and [90.6, 13.0]. For less aggressive faults, that is, with  $R_{f\_max}$ , the PM and BW are equal for the six plants, PM =  $92.4^\circ$ , BW = 3.1 Hz.

## 4 | EXPERIMENTAL RESULTS

In the experimental setup, each inverter in Figure 4 is composed of a 1.9-kVA Guasch MTL-CBI0060F12IXHF full-bridge converter equipped with an LCL output filter. An AMREL SPS800-12-D013 DC source emulates the primary power source of each DG. Each node has its own DSP to run the controller—a dual core Texas Instruments F28M36 floating point DSP. The reference voltage  $v^*$ , obtained by the control shown in Figure 5, is used in the output voltage loop to calculate the current references. These references are processed in the inner current loop that provides the switching signals through a SVM [1]. Table 2 lists the main parameters of the system.

In the load, the overcurrent is produced by connecting a low value resistor  $R_f$  between phase  $a$  and phase  $b$  during a short lap of time, 0.3 s, and it is cleared by disconnecting the resistor between lines. When the resistor connected between lines has a value of zero, an extremely high current is demanded to the nearest DGs. In this case, in the experimental setup, these DGs are immediately disconnected by the overcurrent built-in protection scheme. Thus, in the first test,

when demonstrating the system without the proposed control, a  $R_f$  resistor of  $2 \Omega$  is used. This value produces a lower overcurrent compared with the one produced by a real short circuit between lines. In this case, the currents reach values below the disconnection threshold of the DGs. The short circuit is produced just in the global load node (bus 4), see Figure 4, being DG #4 the nearest generation unit.

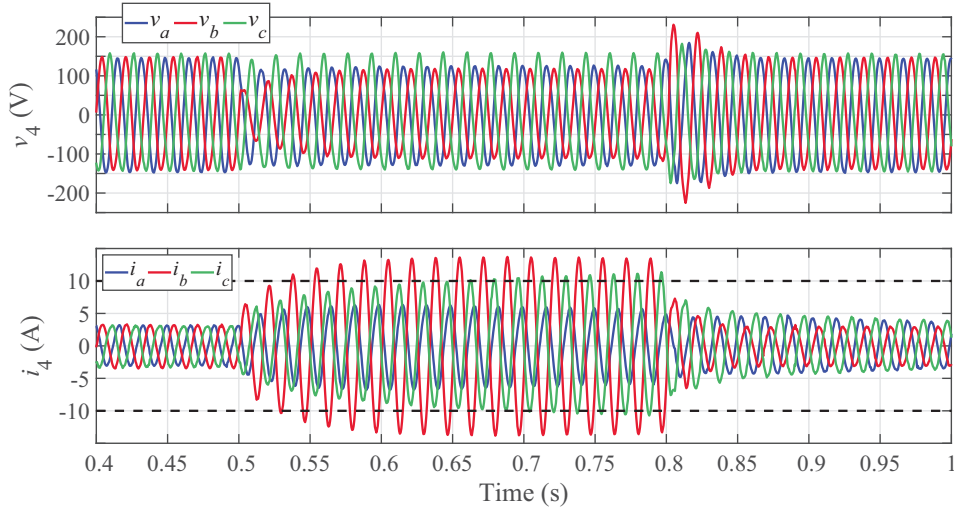
### 4.1 | Response to short circuit without current limitation

Figure 10 shows the phase voltages (top) and currents (bottom) measured at the output of node #4 when the proposed current limiting control is not activated and the

short-current appears at  $t = 0.5$  s. An unbalanced voltage sag is produced, being phase  $b$  the most affected by the disturbance. When the fault is cleared, the voltages suffer an overshoot that brings the phase  $b$  amplitude to a maximum value. Also the DG #4 currents are highly affected by the fault, phase  $b$  being the most perturbed phase which reaches a maximum value of 13.5 A, which is obviously higher than the

maximum allowable current  $I_{rated} = 10$  A. In a conventional practical operation, the overcurrent protection algorithm must disconnect the generator or alternatively clamp this current to a maximum of 10 A, which will produce distortion. It must be noted that, after the fault is cleared at  $t = 0.8$  s, the current experiences a transient until it returns to a steady state (0.5 s in this case as can be seen in the next figure).

Figure 11 shows the per unit (p.u.) RMS phase voltages (top plots) and phase currents (bottom plots) in each generation node ( $V_1$  to  $V_6$  and  $I_1$  to  $I_6$ ) when the current limiting control is not activated. The top figures show the phase voltages before the fault (first 0.5 s), during the fault, and 0.5 s after the fault clearance. The short circuit produces an unbalanced voltage sag, being node #4 the most affected, as expected, where



**FIGURE 10** Node #4 phase voltages (top) and phase currents (bottom) when the maximum current control is not activated,  $R_f = 2 \Omega$

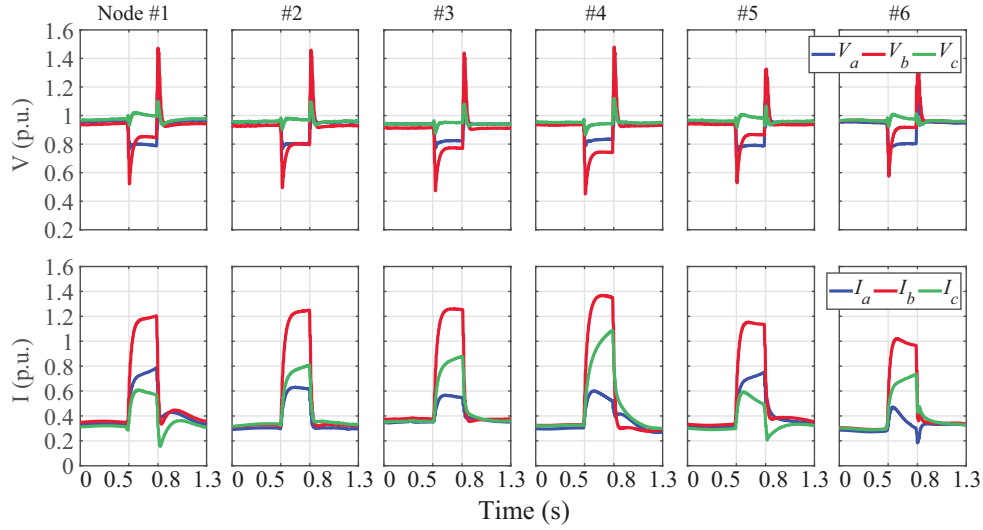


**FIGURE 11** DGs phase voltages (top) and phase currents (bottom) when the proposed maximum current control is not activated,  $R_f = 2 \Omega$

phase  $b$  voltage is reduced to 0.74 p.u. compared with roughly 0.95 p.u. during a normal operation. None of the voltages during a normal operation are at 1 p.u. due to the inherent voltage drop caused by the reactive power droop Equation (2). Obviously, the adverse effects of the fault are naturally mitigated at the farthest nodes to the load. To see this fact, compare for example the voltages and currents in nodes #1 and #6 to the values at #4.

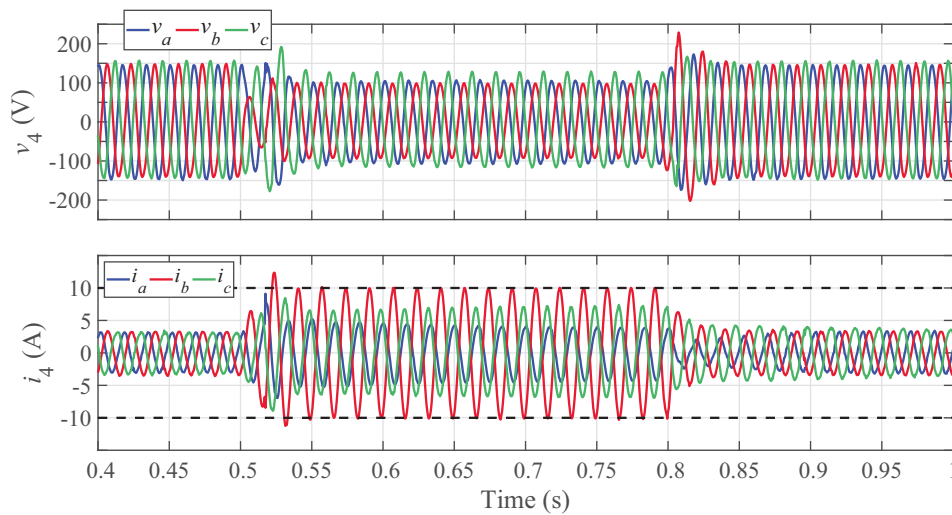
## 4.2 | Response to short circuit with maximum current injection

Figure 12 shows the phase voltages and currents measured at node #4 when the proposed current-limiting control is activated. As can be seen, one of the phase currents is set to the  $I_{rated}$  threshold as desired, with a slight initial overshoot

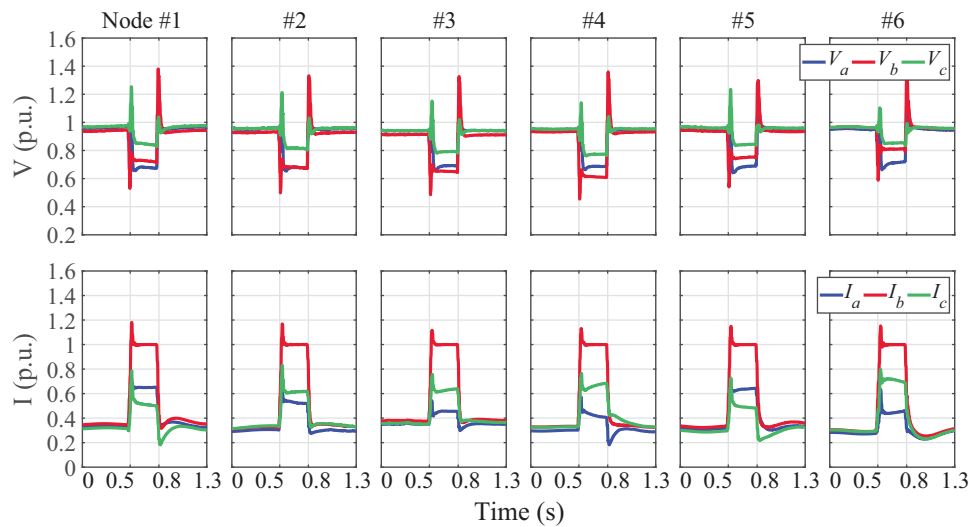
Also, it must be observed that, as expected by the nature of the proposed control, during the fault the voltage amplitudes are lower compared to the voltages when no control is applied, see Figure 10. However, this is not a drawback in a short circuit situation, in which the main objective is to protect the inverter and to help the microgrid by injecting the maximum inverter current.

Figure 13 shows the p.u. RMS phase voltages and currents in each generation node with the current limiting control activated. As can be seen, all the injected currents are successfully limited to  $I_{rated}$ , and most importantly for each inverter, one of the phase currents is exactly  $I_{rated}$ .

During the fault, the active power sharing is also ensured by the droop method scheme. Figure 14 shows active power, reactive power and the drooped reference frequency of each DG. The maximum deviation in active power sharing is approxi-



**FIGURE 12** Node #4 phase voltages (top) and phase currents (bottom) when the maximum current control is activated,  $R_f = 2 \Omega$



**FIGURE 13** DGs phase voltages (top) and phase currents (bottom) when the proposed maximum current control is activated,  $R_f = 2 \Omega$

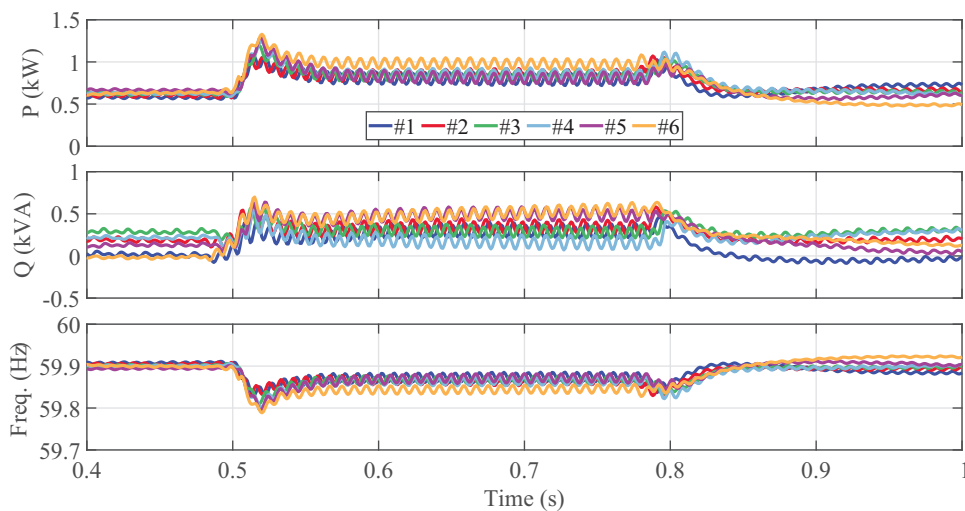


**FIGURE 14** DGs active power, reactive power and reference frequency when the proposed control is activated,  $R_f = 2 \Omega$ , filtered at 12 Hz

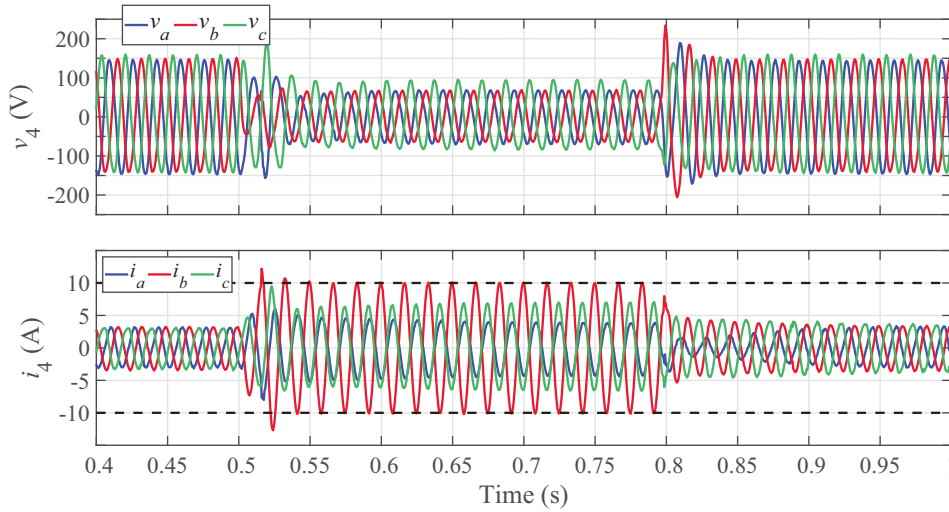


**FIGURE 15** Node #4 phase voltages (top) and phase currents (bottom) when the maximum current control is activated,  $R_f = 0 \Omega$

mately 21%, which can be considered acceptable in such an aggressive situation as a short circuit in the microgrid load. Some power oscillations at  $2\omega_o$ , caused by the unbalanced voltages and currents, can be clearly seen in Figure 14. It is worth mentioning that these oscillations appear during the short circuit with all current limiting methods. Its practical implication is small. Power oscillations cause only small oscillations in the input voltage of the inverter, due to the high capacity of the DC-link capacitor [7, 8].

### 4.3 | Response to severe short circuit

To emulate a worse fault, the test was replicated connecting phases  $a$  and  $b$  with a short circuit with  $R_f = 0 \Omega$ . In this case, the scenario with the proposed control inactive cannot be shown because all the DGs are disconnected immediately by the overcurrent protection scheme. However, when the control is activated, the currents are safely limited to the desired value.

Figure 15 shows voltages and currents at node #4, and Figure 16 shows voltages and currents at each DG node. A deep voltage sag with some phase voltages below 0.5 p.u. is produced, but even in this case one of the amplitudes of the phase currents is perfectly fixed at 10 A, as desired.

From the previous results, it can be concluded that the proposed control is able to meet the control objective regardless of the severity of the fault. As stated in Section 1, as far as the authors know, state-of-the-art controllers do not achieve this interesting feature.

### 4.4 | Comparison with virtual impedance method

To clearly compare the proposal with the state-of-the-art, the controller in [19] has been implemented as a reference, adding a

virtual output resistance  $R_p = 12 \Omega$  during the overcurrent. This value has been calculated to provide a current of 1 p.u. during the most severe short circuit, that is,  $R_f = 0 \Omega$ . The experimental setup shown in Figure 4 has been used for this new test with only five DG working (#1 to #5), in order to slightly change the system topology and demonstrate that the proposal is still valid. To make the comparison easy, only the voltages and currents of one node are represented in the figures. Three different short circuits have been tested, using three different fault resistors  $R_f = 0 \Omega$ ,  $2 \Omega$  and  $4 \Omega$ .

When testing the system with  $R_f = 0 \Omega$ , Figure 17b shows that the reference control works perfectly with this severe short circuit, due to the fact that the maximum current is 1 p.u. In this case, there is a severe drop in phase  $a$  voltage, with the phase voltages becoming highly unbalanced (high negative-sequence voltage). The proposed control behaviour is shown in Figure 17a, where the maximum current is also at 1 p.u. but

with the three phases suffering almost the same voltage drop, which produces a low negative-sequence voltage, as desired.

With less severe short circuits the superiority of the proposal can be clearly seen. The most important point is that the maximum current is always 1 p.u. with the proposal (see Figures 17c and 17e). With the reference controller the maximum current decreases as the short circuit resistor increases (see Figures 17d and 17f). In addition, the negative-sequence voltage is smaller using the proposal, as shown in these results.

## 5 | CONCLUSION

Overcurrents are particularly challenging in islanded microgrids with a high penetration of inverter-based grid-forming nodes. Contrary to synchronous generators, inverter-based grid-forming nodes cannot deal with high overcurrents without compromising the voltage quality and stability. Different works have dealt with the requirement of limiting the output cur-

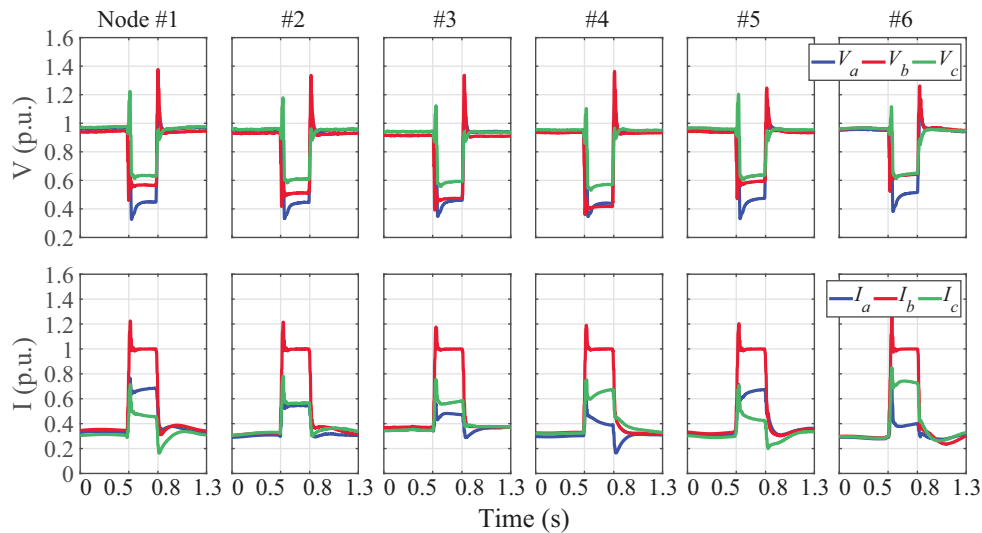


**FIGURE 16** DGs phase voltages (top) and phase currents (bottom) when the proposed maximum current control is activated,  $R_f = 0 \Omega$

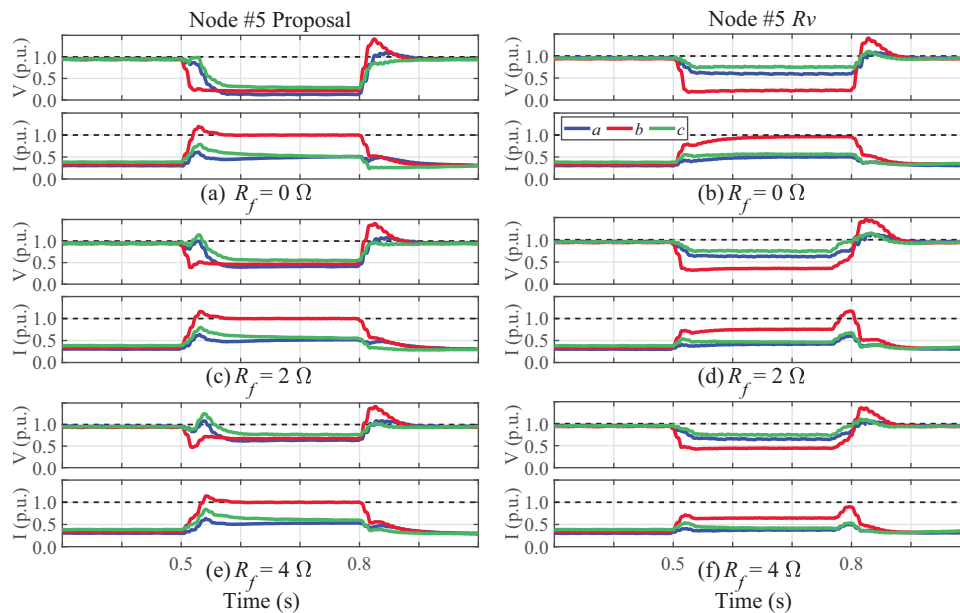


**FIGURE 17** DG #5 phase voltages and currents for different short circuits. Left column: results from the proposed control, right column: results from the reference control

rent in the converters operating as voltage sources that ensure the power quality in an islanded microgrid. However, the very prominent feature of providing maximum current injection in these challenging circumstances is not ensured. This work has proposed a closed-loop controller that ensures maximum current injection during any kind of fault in all the grid-forming nodes of an islanded microgrid. Also, the voltage control loop is fully functional, in order to support the power quality collaboratively between the grid-forming nodes. A mathematical model of the faulted system has been presented. The system model has allowed us to identify the control variables that limit the maximum current, whereas the virtual impedance was the one used

most frequently in previous works. However, the proposed control has been based on modifying the amplitude of the reference voltage (another of the control variables identified in the model) to reduce the current during short circuits and to fix it to the rated current of the system. Based on this control objective, the controller configuration has been derived using  $H_\infty$  techniques, thus guaranteeing a stable operation for all grid-forming nodes.

## AUTHOR CONTRIBUTIONS

Jaume Miret: Conceptualization; Writing—original draft; Writing—review & editing. Manel Velasco: Methodology; Resources.



## ACKNOWLEDGEMENTS

This work is part of the project I+D+i PID2021-122835OB-C21, financed by Ministry of Science, Innovation and Universities of Spain MCIN/AEI/10.13039/501100011033 and by the European Regional Development Fund, FEDER 'Una manera de hacer Europa'.

## CONFLICT OF INTEREST

The authors declare no conflict of interest.

## DATA AVAILABILITY STATEMENT

The data that support the findings of this study are available from the corresponding author upon reasonable request.

## ORCID

Jaume Miret  <https://orcid.org/0000-0003-1175-4900>

Miguel Castilla  <https://orcid.org/0000-0002-3284-860X>

## REFERENCES

- Blaabjerg, F., Teodorescu, R., Liserre, M., Timbus, A.V.: Overview of control and grid synchronization for distributed power generation systems. *IEEE Trans. Ind. Electron.* 53(5), 1398–1409 (2006)
- IEEE Application Guide for IEEE Std 1547: IEEE Standard for Interconnecting Distributed Resources with Electric Power Systems, IEEE Std. 1547.2-2008 (2009)
- Resolution-P.O.12.3-Response requirements against voltage dips in wind installations. Red Electrica, March (2006) [www.rec.es](http://www.rec.es) (translated to English by Spanish Wind Association AEE [www.aeolica.es](http://www.aeolica.es))
- Tsili, M., Papathanassiou, S.: A review of grid code technical requirements for wind farms. *IET Renew. Power Gen.* 3(3), 308–332 (2009)
- Islam Sarkar, M.N., Gunaruwan Meeegahapola, L., Datta, M.: Reactive power management in renewable rich power grids: A review of grid-codes, renewable generators, support devices, control strategies and optimization algorithms. *IEEE Access* 6, 41458–41489 (2018)
- Bollen, M.H.J.: *Understanding Power Quality Problems: Voltage Sags and Interruptions*. IEEE Press, New York (2000)
- Milicua, A., Abad, G., Rodriguez Vidal, M.A.: Online reference limitation method of shunt-connected converters to the grid to avoid exceeding voltage and current limits under unbalanced operation—Part I: Theory. *IEEE Trans. Energy Convers.* 30(3), 852–863 (2015)
- Milicua, A., Abad, G., Rodriguez Vidal, M.A.: Online reference limitation method of shunt-connected converters to the grid to avoid exceeding voltage and current limits under unbalanced operation—Part II: Validation. *IEEE Trans. Energy Convers.* 30(3), 864–873 (2015)
- Camacho, A., Castilla, M., Miret, J., Borrell, A., Garcia de Vicuña, L.: Active and reactive power strategies with peak current limitation for distributed generation inverters during unbalanced grid faults. *IEEE Trans. Ind. Electron.* 62(3), 1515–1525 (2015)
- Chen, H.-C., Lee, C.-T., Cheng, P.-T., Teodorescu, R., Blaabjerg, F.: A low-voltage ride-through technique for grid-connected converters with reduced power transistors stress. *IEEE Trans. Power Electron.* 31(12), 8562–8571 (2016)
- Jia, J., Yang, G., Nielsen, A.H.: A review on grid-connected converter control for short circuit power provision under grid unbalanced faults. *IEEE Trans. Power Del.* 33(2), 649–661 (2018)
- Gkountaras, A., Dieckerhoff, S., Sezi, T.: Evaluation of current limiting methods for grid forming inverters in medium voltage microgrids. In: *IEEE Energy Conversion Congress and Exposition*, pp. 1–8 (2015)
- Gkountaras, A., Dieckerhoff, S., Sezi, T.: Development of a short circuit strategy for medium voltage hybrid microgrids. In: *IEEE International Symposium on Power Electronics for Distributed Generation Systems*, pp. 1–8 (2015)
- Bottrell, N., Green, T.C.: Comparison of current-limiting strategies during fault ride-through of inverters to prevent latch-up and wind-up. *IEEE Trans. Power Electron.* 29(7), 3786–3797 (2014)
- Zamani, M.A., Yazdani, A., Sidhu, T.S.: A control strategy for enhanced operation of inverter-based microgrids under transient disturbances and network faults. *IEEE Trans. Power Del.* 27(4), 1737–1747 (2012)
- Li, Z., Hu, J., Chan, K.W.: A new current limiting and overload protection scheme for distributed inverters in microgrids under grid faults. *IEEE Trans. Ind. Appl.* 57(6), 6362–6374 (2021)
- Fariborz Zarei, S., Mokhtari, H., Blaabjerg, F.: Fault detection and protection strategy for islanded inverter-based microgrids. *IEEE J. Emerg. Sel. Topics Power Electron.* 9(1), 472–484 (2021)
- Plet, C.A., Green, T.C.: A method of voltage limiting and distortion avoidance for islanded inverter-fed networks under fault. In: *Proceedings of Europe Conference on Power Electronics and Applications*, pp. 1–8 (2011)
- Salha, F., Colas, F., Guillaud, X.: Virtual resistance principle for the overcurrent protection of PWM voltage source inverter. In: *IEEE PES Innovative Smart Grid Technology Conference*, pp. 1–6 (2010)
- He, J., Li, Y.W.: Analysis, design, and implementation of virtual impedance for power electronics interfaced distributed generation. *IEEE Trans. Ind. Appl.* 47(6), 2525–2538 (2011)
- Paquette, A.D., Divan, D.M.: Virtual impedance current limiting for inverters in microgrids with synchronous generators. *IEEE Trans. Ind. Appl.* 51(2), 1630–1638 (2015)
- Zarei, S.F., Mokhtari, H., Ghasemi, M.A., Blaabjerg, F.: Reinforcing fault ride through capability of grid forming voltage source converters using an enhanced voltage control scheme. *IEEE Trans. Power Delivery* 34(5), 1827–1842 (2019)
- Lu, X., Wang, J., Guerrero, J.M., Zhao, D.: Virtual-impedance-based fault current limiters for inverter dominated AC microgrids. *IEEE Trans. Smart Grid* 9(3), 1599–1612 (2018)
- ang, L., Xin, H., Wang, Z., Zhang, L., Wu, K., Hu, J.: Transient stability analysis and control design of droop-controlled voltage source converters considering current limitation. *IEEE Trans. Smart Grid* 10(1), 578–591 (2019)
- Taul, M.G., Wang, X., Davari, P., Blaabjerg, F.: Current limiting control with enhanced dynamics of grid-forming converters during fault conditions. *IEEE J. Emerg. Sel. Topics Power Electron.* Early Access Article (2019)
- Sadeghkhani, I., Hamedani Golshan, M.E., Guerrero, J.M., Mehrizi-Sani, A.: A current limiting strategy to improve fault ride-through of inverter interfaced autonomous microgrids. *IEEE Trans. Smart Grid* 8(5), 2138–2148 (2017)
- Chen, Z., Pei, X., Yang, M., Peng, L., Shi, P.: A novel protection scheme for inverter-interfaced microgrid (IIM) Operated in Islanded Mode. *IEEE Trans. Power Electron.* 33(9), 7684–7697 (2018)
- Vasquez, J.C., Guerrero, J.M., Miret, J., Castilla, M., Garcia de Vicuña, L.: Hierarchical control of intelligent microgrids. *IEEE Ind. Electron. Mag.* 4(4), 23–29 (2010)
- Li, B., Zhou, L., Yu, X., Zheng, C., Liu, J.: Improved power decoupling control strategy based on virtual synchronous generator. *IET Power Electron.* 10(4), 462–470 (2017)
- Vasquez, J.C., Guerrero, J.M., Savaghebi, M.J., Eloy-Garcia, J., Teodorescu, R.: Modeling, analysis, and design of stationary reference frame droop controlled parallel three-phase voltage source inverters. *IEEE Trans. Ind. Electron.* 60(4), 1271–1280 (2013)
- Guerrero, J.M., Vasquez, J.C., Matas, J., Garcia de Vicuña, L., Castilla, M.: Hierarchical control of droop-controlled AC and DC microgrids - A general approach towards standardization. *IEEE Trans. Ind. Electron.* 58(1), 158–172 (2011)
- Anderson, P.M.: *Analysis of Power Faulted Systems*. John Wiley & Sons, New York (1995)
- Floriduz, A., Tucci, M., Rivero, S., Ferrari-Trecate, G.: Approximate Kron reduction methods for electrical networks with applications to plug-and-play control of AC islanded microgrids. *IEEE Trans. Control Syst. Technol.* 27(6), 2403–2416 (2019)

34. Fortuna, L., Nunnari, G., Gallo, A.: Model Order Reduction Techniques With Applications in Electrical Engineering. Springer, Berlin, Germany (2012)
35. Skogestad, S., Postlethwaite, I.: Multivariable Feedback Control: Analysis and Design. John Wiley & Sons, Hoboken, New Jersey (2005)
36. Zhou, K., Doyle, J.C.: Essentials of Robust Control. Prentice-Hall, Upper Saddle River, New Jersey (1998)
37. Doyle, J.C., Francis, B.A., Tannenbaum, A.R.: Feedback Control Theory. Dover Publications, Mineola, New York (2013)
38. Robles, E., Ceballos, S., Pou, J., Martín, J.L., Zaragoza, J., Ibañez, P.: Variable-frequency grid-sequence detector based on a quasi-ideal low-pass filter stage and a phase-locked loop. IEEE Trans. Power Electron. 25(10), 2552–2563 (2010)

**How to cite this article:** Miret, J., Castilla, M., Velasco, M., Guzmán, R., de Vicuña, L.G.: Maximum current injection method for grid-forming inverters in an islanded microgrid subject to short circuits. IET Power Electron. 1–15 (2022).

<https://doi.org/10.1049/pel2.12448>

## APPENDIX

As an example, the complete modelling of inverter #1 under a severe  $R_f = 0 \Omega$  line  $a$  to line  $b$  fault in Bus 4 is developed. With the inverter #1 impedance-values listed in Table 2 substituted into (7), and then using the transformation (9) to (11), the coefficients of  $Y_{pn}$  in (12) for this inverter and fault are

$$Y_{11}(s) = \frac{-136.9 \cdot (s + 3356.2)}{(s + 68.5) \cdot (s + 6643.8)} \quad (A1)$$

$$Y_{21}(s) = \frac{-10^3 \cdot (225.1 + 390.0 \cdot j)}{(s + 68.5) \cdot (s + 6643.8)}. \quad (A2)$$

The high-frequency poles and zeroes can be removed due to the fact that they are far enough from the working BW

$$Y_{11\_LF}(s) = \frac{-69.2}{s + 68.5} \quad (A3)$$

$$Y_{21\_LF}(s) = \frac{-(33.8 + 58.7 \cdot j)}{s + 68.5}. \quad (A4)$$

**TABLE A1** Set of plants with their gains and poles

Inverter	Index $i$	$k_c R_f = 0$	$\omega_c R_f = 0$	index $i$	$k_c R_f = R_{f\_max}$	$\omega_c R_f = R_{f\_max}$
#1	1	1.7321	68.5	7	0.0645	1861.8
#2	2	1.7321	94.3	8	0.0645	2564.3
#3	3	0.7873	268.3	9	0.0642	3330.2
#4	4	0.7873	333.3	10	0.0642	4137.5
#5	5	0.7873	180.3	11	0.0642	2238.3
#6	6	0.4559	234.5	12	0.0644	1688.1

**TABLE A2** Nominal plant, uncertainty gains and poles

Function	$k_c$	$\omega_c$
$Y_{nominal}$	0.8982	1833
$\omega_\mu^a$	0.8340	2000

Then, the phase current amplitudes are expressed as

$$I_a = \left| \frac{-69.2 - (33.8 + 58.7j) e^{j0}}{s + 68.5} v \right| = \left| \frac{118.5 \angle \theta_a}{s + 68.5} v \right| \quad (A5)$$

$$I_b = \left| \frac{-69.2 e^{-j\frac{2\pi}{3}} - (33.8 + 58.7j) e^{j\frac{2\pi}{3}}}{s + 68.5} v \right| = \left| \frac{118.6 \angle \theta_b}{s + 68.5} v \right| \quad (A6)$$

$$I_c = \left| \frac{-69.2 e^{j\frac{2\pi}{3}} - (33.8 + 58.7j) e^{-j\frac{2\pi}{3}}}{s + 68.5} v \right| = \left| \frac{1.4 \angle \theta_c}{s + 68.5} v \right|. \quad (A7)$$

Finally, the transfer function of the maximum amplitude for inverter #1 under a line  $a$  to line  $b$  short circuit is

$$I_{max} = \frac{118.6}{s + 68.5} V = 1.73 \frac{68.5}{s + 68.5} V = Y_1(s) V. \quad (A8)$$

Following this methodology for the six inverters and for the two extreme short circuit cases ( $R_f = 0 \Omega$  and  $R_f = R_{f\_max} \Omega$ ), a set of 12 plants are all reduced to first-order systems:

$$Y_i(s) = k_{c\_i} \frac{\omega_{c\_i}}{s + \omega_{c\_i}}. \quad (A9)$$

Table A1 shows the values of these 12 plants. From these values, the nominal plant  $Y_{nominal}(s)$  can be obtained, with gain  $k_{c\_nominal}$  being the mean value between the maximum and the minimum values of  $k_{c\_i}$ . The nominal pole  $\omega_{c\_nominal}$  is chosen in order that the nominal plant, at high frequencies, presents higher gain than any other plant of the set. As can be seen in Figure 9, the nominal plant is roughly in the middle of the rest of the plants.

The additive uncertainty model  $\omega_\mu^a(s)$  around the nominal plant must accomplish

$$|\omega_\mu^a(j\omega)| > |Y_i(j\omega) - Y_{nominal}(j\omega)| \quad \forall i, \omega. \quad (A10)$$

that is, it must present a magnitude higher than any of the differences between the plants and the nominal one.

Table A2 lists the gains and poles of the nominal plant and the additive uncertainty.